RESEARCH ARTICLE

[M]acro-
molecular
Materials and Engineering
Open Access
www.mame-journal.de

4D Printing of Magneto-Thermo-Responsive PLA/PMMA/Fe$_3$O$_4$ Nanocomposites with Superior Shape Memory and Remote Actuation

Hossein Doostmohammadi, Majid Baniassadi, Mahdi Bodaghi,* and Mostafa Baghani*

This study presents the development and 4D printing of magnetic shape memory polymers (MSMPs) utilizing a composite of polylactic acid (PLA), polymethyl methacrylate (PMMA), and Fe$_3$O$_4$ nanoparticles. The dynamic mechanical analysis reveals that the integration of Fe$_3$O$_4$ maintains the broad thermal transition without significantly affecting α-relaxation time, indicating high compatibility and homogeneous distribution of the nanoparticles within the polymer matrix. Field emission scanning electron microscopy further confirms the high compatibility of PLA and PMMA phases as well as uniform dispersion of Fe$_3$O$_4$ nanoparticles, essential for the effective transfer of heat during the shape memory process. Significantly, the incorporation of magnetic nanoparticles enables remote actuation capabilities, presenting a substantial advancement for biomedical applications. 4D-printed MSMP nanocomposites exhibit exceptional mechanical properties and rapid, efficient shape memory responses under both inductive and direct heating stimuli, achieving 100% shape fixity and 100% recovery within ≈85 s. They are proposed as promising candidates for biomedical implants, specifically for minimally invasive implantation of bone scaffolds, due to their rapid remote actuation, biocompatibility, and mechanical robustness. This research not only demonstrates the 4D printability of high-performance MSMPs but also introduces new possibilities for the application of MSMPs in regenerative medicine.
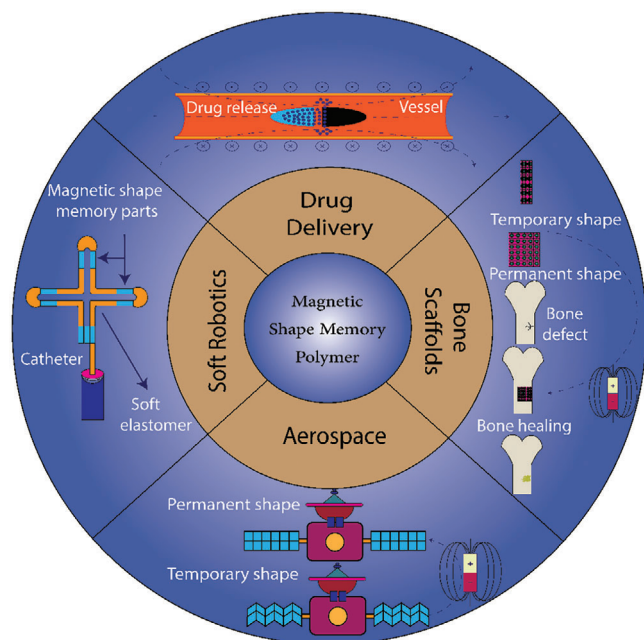
H. Doostmohammadi, M. Baniassadi, M. Baghani
School of Mechanical Engineering
College of Engineering
University of Tehran
Tehran 1417614411, Iran
E-mail: baghani@ut.ac.ir
M. Bodaghi
Department of Engineering
School of Science and Technology
Nottingham Trent University
Nottingham NG11 8NS, UK
E-mail: mahdi.bodaghi@ntu.ac.uk

1. Introduction

Smart materials are a fascinating category of materials in which one or more properties can be changed in response to an external stimulus like light, heat, electromagnetic fields, moisture, PH, some chemicals, etc.[1–7] Among smart materials, shape memory polymers are able to change their size, shape, or stiffness when exposed to an external stimulus. Researchers have conducted many experiments concerning the response of different compounds to different stimuli.[8–11] Most of these studies have investigated the shape recovery of polymers by means of direct heating.[12–18] However, in recent years, restrictions in specific applications (as shown in **Figure 1**) have drawn the attention of scholars to other forms of stimulating—chiefly remotely—shape memory effect (SME).[19–27] Magnetic shape memory polymers (MSMPs) are composed of thermo-sensitive polymers and magnetic particles (nano/micron-sized) which can be remotely activated and controlled and are highly ideal to be used in biomedical fields due to their low cost and ability to be easily processed into any desired shape. They can be implanted inside the human body where direct heating can harm muscles and vulnerable organs. In fact, MSMPs are activated by utilizing an inductive heating approach.[28] Induction heating is a contactless technique to transfer heat via an induction coil to the magnetic particles incorporated inside the polymer matrix. **Figure 2** shows the mechanism of induction heating. The induction heating occurs when high-frequency alternating current (AC) is conducted via an electromagnet. The magnetic field permeates through the nanocomposite sample inducing the eddy currents within the conductor. The eddy currents passing through the material, face resistance, and subsequently heat generation occurs (Joule heating).[29] The magnetic energy that is required to heat up the magnetic nanoparticles has been calculated by Davidson et al.,[30] but according to his findings based on Hergt et al [31] and Rosensweig et al.'s studies,[32] frequencies of 100 kHz and above are strong enough to heat up superparamagnetic nanoparticles. Researchers have employed nickel zinc ferrite, Ni-Me-Ga powders, and predominantly iron oxide as the primary magnetic fillers in MSMPs.[33–35] Mohr et al.[36] carried out research on remote activation of nanocomposites consisting

ADVANCED
SCIENCE NEWS
www.advancedsciencenews.com

|M acro-
olecular
Materials and Engineering
Open Access

www.mame-journal.de

Figure 1. Applications of MSMPs.

of Cycloaliphatic TFX as the matrix and Fe3O4 nanoparticles as magnetic fillers. The samples were placed in an AC magnetic field with f = 298 kHz and recovered their permanent shape in 22 seconds. Yakacki et al.[37] studied the effect of magnetic particle content on the recovery time of the polymers. Their investigation revealed that an increase in the amount of Fe_3O_4 correlates with a rise in heating rate and is accompanied by a decrease in the ductility of the structure. Puig et al.[38] performed research on the magnetic shape memory effect of an epoxy-based magnetic nanocomposite. Despite the aggregation of magnetic nanoparticles within the polymeric matrix, the samples with an 8% weight ratio (wt.) of Oleic acid (OA) coated magnetite nanoparticles exhibited full shape recovery. This aggregation suggests that the dispersity of nanoparticles was not enhanced by the alkyl chains of OA.
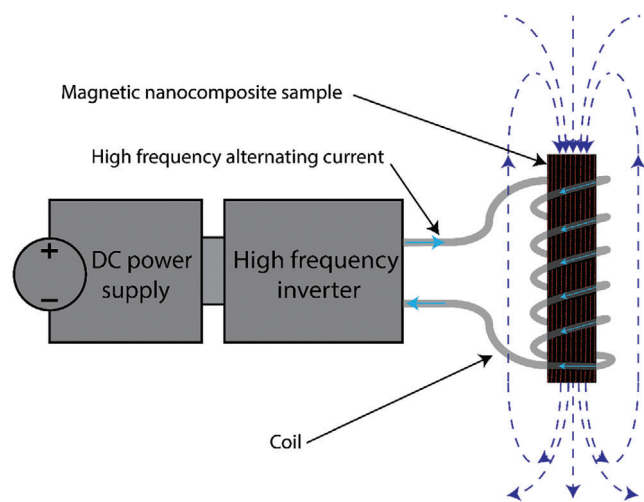
Figure 2. Schematic of inductive heating in MSMPs.

While thermosets are more frequently used for their shape memory properties due to the crosslinking components,[39] thermoplastics can also show a great shape memory effect when they exhibit crystallinity or when they are blended with another polymer. In thermoplastic blends, the two-phased morphology is responsible for the shape memory effect of the materials. The rigid amorphous regions in thermoplastic blends serve as alternatives to the hard segments found in thermosets.[40] When chemical crosslinking is not possible, the entanglement and bonding between two different polymer chains can play the role of crosslinking. This phenomenon is also known as physical crosslinking. In addition to that, the ease of manufacturing, cost-effectiveness, and recyclability are considered as the advantages of thermoplastics over thermosets.

The recent rapid and significant advances in additive manufacturing techniques have allowed the production of multiple structures in various scales for diverse industries and applications.[41] The applications of 3D printing are of a wide range (including biomedical implants, bone scaffolds and soft tissues, prototyping and mass production, automotive industries, etc.). Additive manufacturing techniques can be utilized for many types of materials but in the case of smart materials, 3D printing plays a transformative role which is mostly known as 4D printing.[41] The term "4D" refers to the ability of the 3D printed objects to transform to a predictable shape in response to an external stimulus.[42] Biodegradable thermoplastics have been widely used due to their sustainability and the environmental need for reduction in plastic pollution. Polylactic acid (PLA) is an interesting biodegradable material among aliphatic polyesters that has been extensively studied as it has good mechanical properties and great processability.[43,44] In spite of its strength, it possesses low heat distortion, poor impact strength, and low shape recovery. In order to overcome these weaknesses and broaden its range of applications, scientists blend PLA with other thermoplastics to obtain the desired properties.[44–46] Among thermoplastics, poly methyl methacrylate (PMMA) is a great choice to melt-blended with PLA, owing to the high degree of entanglement that can form between their chains.[47] In previous studies,[48,49] it has been noticed that PLA/PMMA blend with 50/50 wt. creates a partial co-continuous morphology and hence, they exhibit great shape memory properties as well as good mechanical strength. To determine the shape memory effect of PLA/PMMA blends with different weight ratios in the study conducted by Samuel et al.,[48] dual shape memory tests were conducted. They observed that in symmetric compounds (50/50 wt. of PLA/PMMA) the switch temperature (the temperature at which the shape switches from temporary to original) and stretching temperature shifted from 70 to 90 °C and 65 to 94 °C, respectively, with high shape fixity ratio (99%) and shape recovery ratio (90%), whereas the asymmetric compounds with 30 wt% and 80 wt% of PMMA exhibit shape recovery ratios less than 80%. Additionally, triple shape memory tests were carried out with fixing temporary shapes at 94 and 65 °C. In all symmetric samples, 60% shape recovery for the first shape and higher than 90% shape recovery for the second shape were documented. In Eshkaftaki et al.'s work,[49] PLA/PMMA polymers with 2 parts per hundred resin/rubber (phr) of graphene nanoplatelets (GNP) displayed a triple shape memory effect with 96.6% of shape recovery. It was noted that the addition of GNP increased the crystallinity of

**ADVANCED
SCIENCE NEWS**

www.advancedsciencenews.com

Macro-
molecular
Materials and Engineering

www.mame-journal.de

Table 1. The properties of Fe_3O_4 nanoparticles.

Purity	99.5%	Size [nm]	15–20
Morphology	Spherical	Color	Dark brown
Bulk density [g cm^{-3}]	≈0.85	True density [g cm^{-3}]	4.8–5.1

PLA and had a direct influence on the shape fixity ratio of the nanocomposites.

Despite the remarkable shape memory properties of PLA/PMMA blends (as mentioned above), previous studies have relied on conventional methodologies requiring direct stimulus for actuation. These approaches can cause intrinsic challenges in biomedical applications where accessibility is constrained, or invasive procedures are to be avoided. Additionally, 3D printing of PLA/PMMA blends remained unexplored since creating filaments from the material was highly challenging due to the presence of PMMA. To address these academic gaps in the literature, in this study, Fe_3O_4 nanoparticles were incorporated in PLA/PMMA blends (50/50 wt.) for the first time due to their superparamagnetic properties to create MSMPs that can be triggered remotely in alternating magnetic fields. These MSMPs were successfully 4D printed by employing a biopellet-based 3D printer. After determining 3D printing parameters, the thermomechanical properties of the additively manufactured specimens were examined by dynamic mechanical thermal analysis (DMTA). The mechanical strength of the specimens was evaluated by tensile testing and as the main part, the shape memory effect of the specimens was assessed by employing direct heating and inductive heating techniques as stimuli. Finally, a potential application for the proposed MSMPs has been introduced.

2. Experimental Section

2.1. Materials

Poly ʟ-lactic acid (PLLA) filament ($\rho = 1.23$ g cm^{-3}, melt flow rate = 6 g/10 min) and poly methyl methacrylate (PMMA) granules ($\rho = 1.19$ g cm^{-3}, melt flow rate = 3.8 g/10 min) were purchased from Guangzhou YOUSU and CHIMEI respectively, Tetrahydrofuran (THF) lab grade (M = 72.11 g mol^{-1}) was purchased from Millipore Sigma and dry PVP coated Fe_3O_4 nanopowder was supplied by US Research Nanomaterials Inc. The properties of Fe_3O_4 nanoparticles are given in **Table 1**.
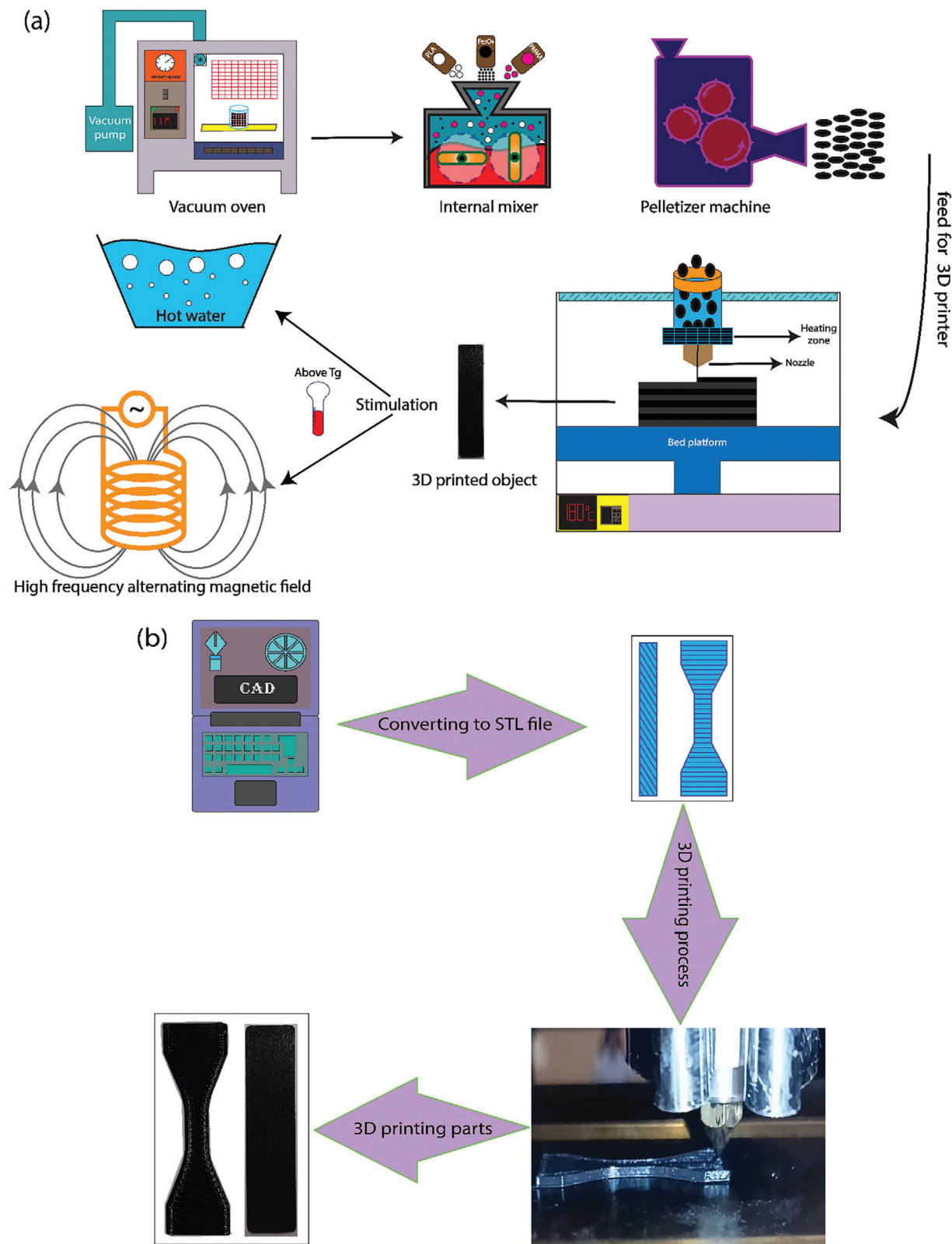
2.2. Processing and 3D Printing

PLA filament was chopped into granules by a pelletizer machine, then PLA and PMMA granules were kept in an oven under vacuum condition for 8 h at 80 °C to remove the moisture and unpolymerized monomers. For fabrication of PLA/PMMA blends, PLA granules were first added to a twin-screw internal mixer (Baopin Technology Co.) at 180 °C for 2 minutes. Then, PMMA granules (50 wt%) were fed and the mixing process continued for 16 min (18 min in total). For the fabrication of PLA/PMMA/ Fe_3O_4, the same procedure was followed but after 10 min of mixing time, Fe_3O_4 particles (with 10 wt%, 12 wt%, and

15 wt%) were added to the mixture and the mixing process continued for 5 more minutes (15 min in total). After that, samples were molded utilizing a hot compression-molding technique at 200 °C for 3 min. Molded sheets were immersed in liquid Nitrogen immediately following the hot compression-molding procedure to prevent cold crystallization of PLA. Although PLA exhibited low crystallinity, even a low level of crystallinity does not allow the chains to fully interact with PMMA chains and therefore it affects the expected co-continuous morphology. The prepared sheets were then chopped into small pieces so that biopellet-based 3D printer (Chakad, CSS1) could process them. **Figure 3a,b** displays the fabrication process of the nanocomposites, 3D printing process, and printed parts, respectively. Similarly, PLA filaments underwent the same procedure, ensuring that they could be examined under identical circumstances. To enhance printability, commercial PLA filaments are usually modified with additives. For purification, the filaments were chopped into small pieces and added to the internal mixer at 190 °C for 5 min. It should be noted that PMMA was not 3D printed due to poor layer adhesion and its high printing temperature (≈240 °C). The investigation into determining 3D printing parameters began with conducting print tests within the range of printing parameters recommended by the PLA filament manufacturer. A total of 25 specimens for the shape memory test and tensile test were 3D printed, and parameters such as bed temperature, nozzle temperature, printing speed, and raster angle were adjusted for each material. The nozzle temperature for PLA/PMMA specimens was higher than for pure PLA due to the lower flowability of the material. The presence of Fe_3O_4 nanoparticles had a similar impact, but they should be printed at temperatures between those of pure PLA and PLA/PMMA because these nanoparticles tend to agglomerate at higher temperatures. Printing speed and bed temperature were progressively studied until printing defects, such as poor layer adhesion, were minimized, and raster angles were selected based on the performance of samples in the shape memory tests and tensile tests. The 3D printing parameters are detailed in **Tables 2** and **3** for the shape memory tests and tensile tests, respectively.

2.3. Characterization

The shape-changing behavior of shape memory polymers (SMPs) is closely linked to the thermal transitions observed in polymers. The glass transition temperature (T_g) represents the main thermal transition range where the segmental motion of polymer chains takes place. Below this temperature, polymers display a glassy state, while in temperatures above it, they reveal rubbery characteristics. It influences the shape memory effect since at $T > T_g$ chains have the freedom to change their configurations. DMTA is employed to Investigate these physical characteristics of polymers. This analysis measures the mechanical properties of the specimens as a function of time, temperature, and frequency. To identify the viscoelasticity and thermomechanical behavior of polymers by DMTA, DMA Q850 from TA instrument was employed. All samples for DMTA analysis were 3D printed into rectangular shapes with dimensions of $25 \times 10 \times 1$ mm^3. Tests were conducted in tensile mode at f = 1 Hz with a heating rate of 5 °C min^{-1}. Glass transition temperature domain can be seen

Figure 3. The process of a) fabricating MSMPs and b) 3D printing process and 3D printing samples for shape memory tests and tensile tests.

ADVANCED
SCIENCE NEWS

www.advancedsciencenews.com

macro-
molecular
Materials and Engineering
Open Access

www.mame-journal.de

Table 2. 3D printing parameters of samples for shape memory test.

Material	Printing speed [mm min^{-1}]	Nozzle temperature [°C]	Raster angle [°]	Bed temperature [°C]
PLA/PMMA (50 wt%)	400	190	0/90	40
PLA/PMMA/Fe$_3$O$_4$ (10%)	300	185	30/−30	50
PLA/PMMA/Fe$_3$O$_4$ (12%)	300	185	30/−30	50
PLA/PMMA/Fe$_3$O$_4$ (15%)	300	185	30/−30	60

Table 3. 3D printing parameters of samples for tensile test.

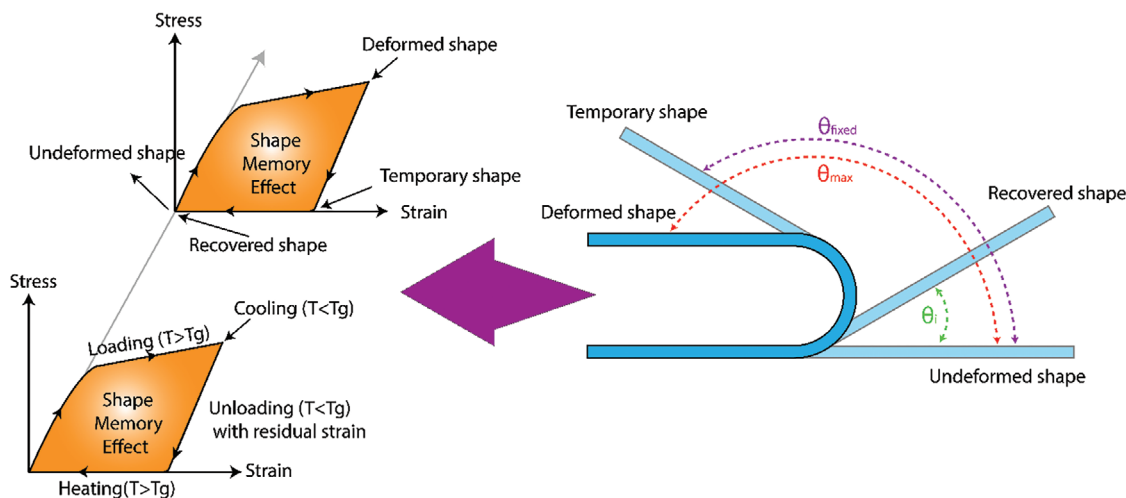| Material	Printing speed [mm min^{-1}]	Nozzle temperature [°C]	Raster angle [°]	Bed temperature [°C]
PLA/PMMA (50 wt%)	400	190	0/90	40
PLA/PMMA/Fe$_3$O$_4$ (10%)	300	185	0/90	50
PLA/PMMA/Fe$_3$O$_4$ (12%)	300	185	0/90	50
PLA/PMMA/Fe$_3$O$_4$ (15%)	300	185	0/90	60

in storage modulus curves when the storage modulus of the material drops dramatically. Tensile tests were performed to study the mechanical properties of the nanocomposites using SANTAM STM-05. The samples were 3D printed according to ASTM D638 type V standard; however, the clamping area was reduced to 10 mm due to the gripper limitations of the device. The characterization and morphological analysis of polymers cannot solely be evaluated through DMTA. Hence, a supplementary analysis is required to support thermomechanical analysis. In many research studies, field emission scanning electron microscopy (FESEM) is carried out utilizing TESCAN Mira 3 to confirm DMTA results. For this analysis, rectangular samples with dimensions of 10 × 10 × 1 mm^3 were 3D printed. EDX mapping analysis was also carried out to reveal the dispersity of Fe$_3$O$_4$ on the surface of the samples. PLA/PMMA samples were etched using THF solvent for 45 min to partially dissolve PMMA phase (3D printed samples would have failed if the time had been extended). Shape memory effect of the 3D printed specimens was studied in both a high-frequency alternating magnetic field and hot water. The hot programming procedure has been chosen for the programming steps. First, the 3D printed samples were heated up to 95 °C (the temperature above the glass transition region), then an external force was employed to bend the samples into U shapes (temporary shapes), and finally, the temporary shapes were locked by cooling the samples down to the room temperature. For stimulation by induction heating, 3D printed parts were placed in a high-frequency alternating magnetic field setup which was capable of providing frequency of f = 100 kHz to f = 150 kHz. For direct heating stimulation, specimens were placed in hot water at 90 °C. In this paper, the shape memory characteristics of the samples were evaluated by shape recovery ratio (R_r) and shape fixity ratio (R_f). These two factors can be calculated by the equations given below:
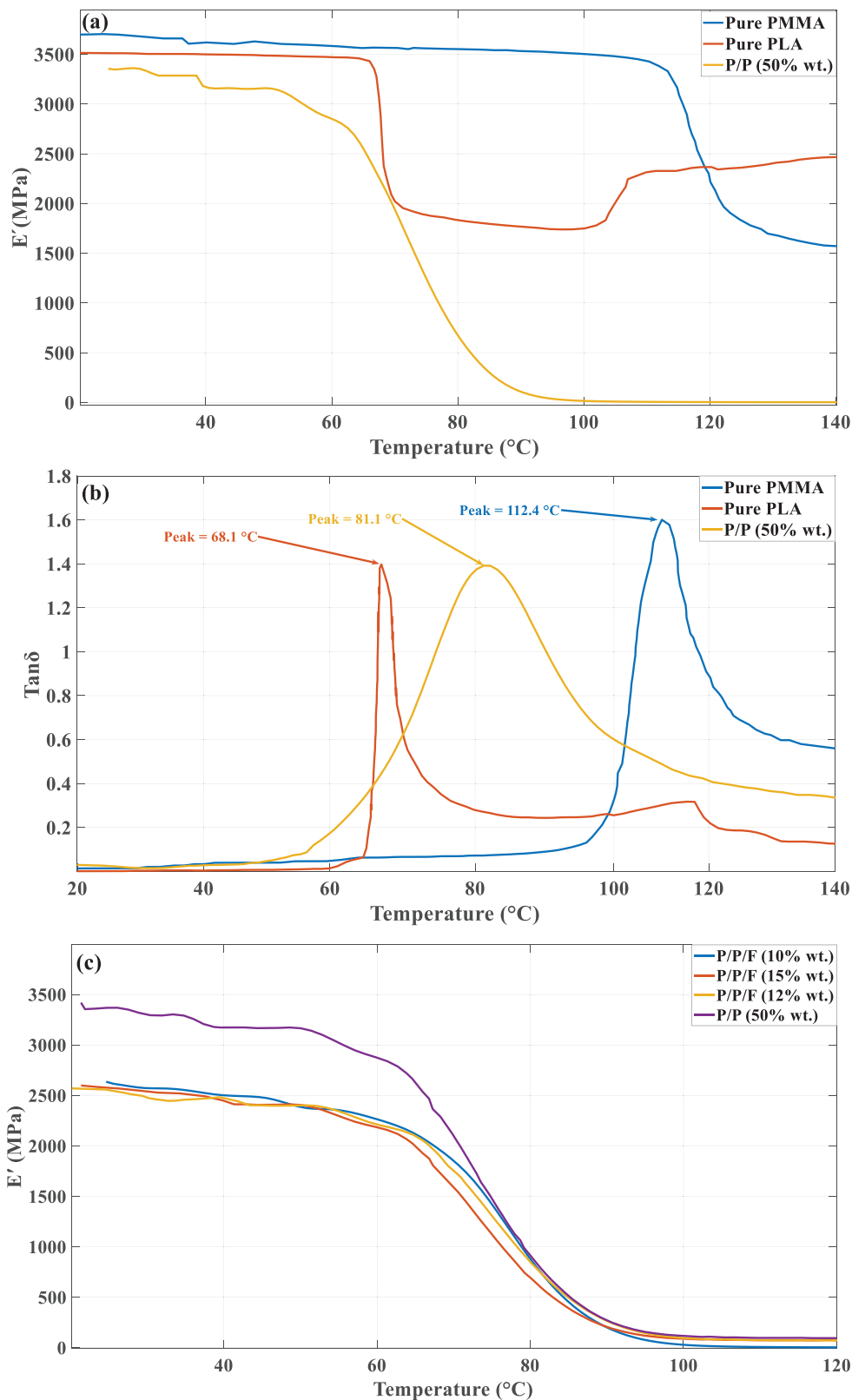
$$R_f = \frac{\theta_{fixed}}{\theta_{max}} \times 100\% \tag{1}$$

$$R_r = \frac{\theta_{max} - \theta_i}{\theta_{max}} \times 100\% \tag{2}$$

As shown in **Figure 4**, θ_{max} is the desired angle for shape fixing, θ_{fixed} is the fixed angle after removing the constraints and θ_i is the unrecovered angle.

Figure 4. Schematic of shape memory thermomechanical test in bending mode.

**ADVANCED
SCIENCE NEWS**

www.advancedsciencenews.com

acro-
olecular
Materials and Engineering
Open Access

www.mame-journal.de

Figure 5. Storage modulus and tanδ curves for a,b) pure samples and PLA/PMMA composites and c,d) MSMPs.

**ADVANCED
SCIENCE NEWS**

www.advancedsciencenews.com

[M] **acro-
olecular
Materials and Engineering**
Open Access

www.mame-journal.de

3. Results and Discussion

3.1. DMTA Results and Thermomechanical Behavior of the Specimens

Figure 5a,b demonstrates DMTA results for pure PLA, pure PMMA, and PLA/PMMA (50/50 wt%), and Figure 5c,d shows DMTA results for nanocomposites with Fe_3O_4 (10 wt%, 12 wt%, and 15 wt%). The storage modulus curve for PLA demonstrates α-relaxation between 65 and 76 °C that is confirmed by the narrow peak of $\tan\delta$ curve. It is also evident that PLA chains start to fold and crystallize when the sample is heated below the melting point. This phenomenon occurs in PLA and is known as cold crystallization. As observed, PLA/PMMA blends exhibit a broad thermal transition ranging from 60 to ≈90 °C. This broadness suggests that the individual chain movements take longer time, owing to the complete entanglement of PLA and PMMA chains. This broadness makes them suitable for multi-shape memory applications but it should be noted that such applications are not the focus of this study. Additionally, cold crystallization is absent in this curve, a result of the processing step involving the placement of the samples in liquid nitrogen, effectively eliminating PLA crystallinity. This assisted in creating a strong bond with PMMA chains which consequently prevented cold crystallization during the analysis. Furthermore, the single transition in storage modulus of polymers indicates that the two polymers are either miscible or highly compatible This can be confirmed by supplementary tests like FE-SEM. It can also be seen in Figure 5c,d that the addition of Fe_3O_4 at any wt. does not affect the broadness of glass transition region. It is also demonstrated that nanocomposites with 10 wt% of nanoparticles have only shifted the glass transition temperature from 81.1 to 82.6 °C. This is due to the well-dispersity of the nano-sized particles and therefore, they do not have a substantial impact on T_g as the micron-sized particles can have; However, the storage modulus of the nanocomposites is 28% lower than PLA/PMMA blends that is due to the partial agglomeration of nanoparticles causing stress concentration within the material.

In order to see the effect of nanoparticles on chain mobility and viscosity of the materials, melt flow rate tests were carried out and according to **Figure 6**, the melt flow rate of magnetic composites displayed lower values compared to PLA/PMMA (50/50 wt%). The slight change in viscosity is due to the following factors. First, the interaction between nanoparticles and the polymer matrix restricts the mobility of the chains, particularly in polymer blends with more than one component. However, the good dispersion of the nanocomposites and the possible water absorption on the Fe_3O_4 nanoparticle surface prevents a significant increase in the viscosity of the nanocomposites. Also, processing conditions, such as the blending process described in the paper, can influence the viscosity as increased crystallinity generally raises viscosity. Therefore, the crystallinity reduction during the blending process helped viscosity changes be controlled in nanocomposites.

3.2. FE-SEM

The morphological analysis of the samples has been conducted utilizing FE-SEM to capture microscopic images. **Figures 7** and **8**
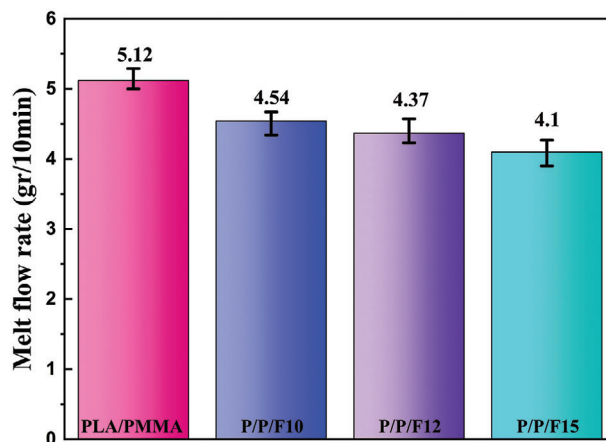

Figure 6. The melt flow rate of nanocomposites.

provide information about FE-SEM analysis of the PLA/PMMA composite and the MSMPs respectively. The etched holes and etched paths in Figure 7 represent PMMA phase in PLA/PMMA blend. As it can be seen, PMMA and PLA phases are highly interconnected. This partial co-continuous morphology leads to enhanced mechanical properties and highly resists to crack propagation. Figure 8a–c includes FE-SEM images along with EDX mapping analysis that show the dispersity of Fe_3O_4 nanoparticles in the nanocomposite materials. These Images confirm Uniform dispersity of nanoparticles inside the polymer matrix. The uniform dispersity ensures the nanoparticles are interconnected and therefore, heat transfers effectively throughout the nanocomposite materials. It also should be noted that well dispersion of the nanomagnetic particles along with the slight changes in viscosity
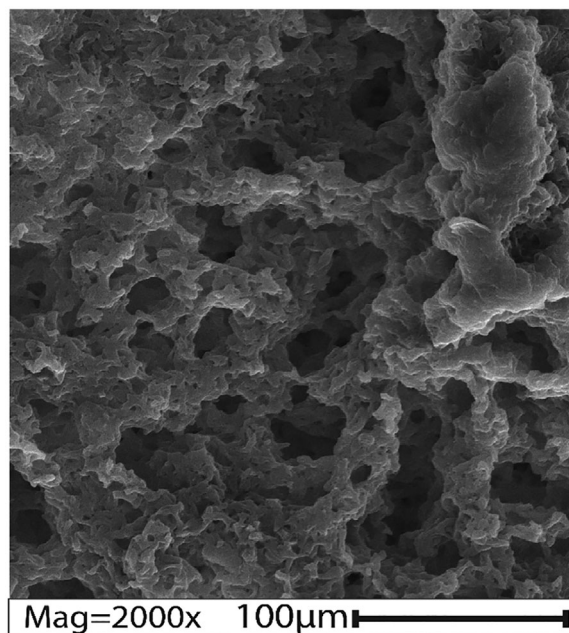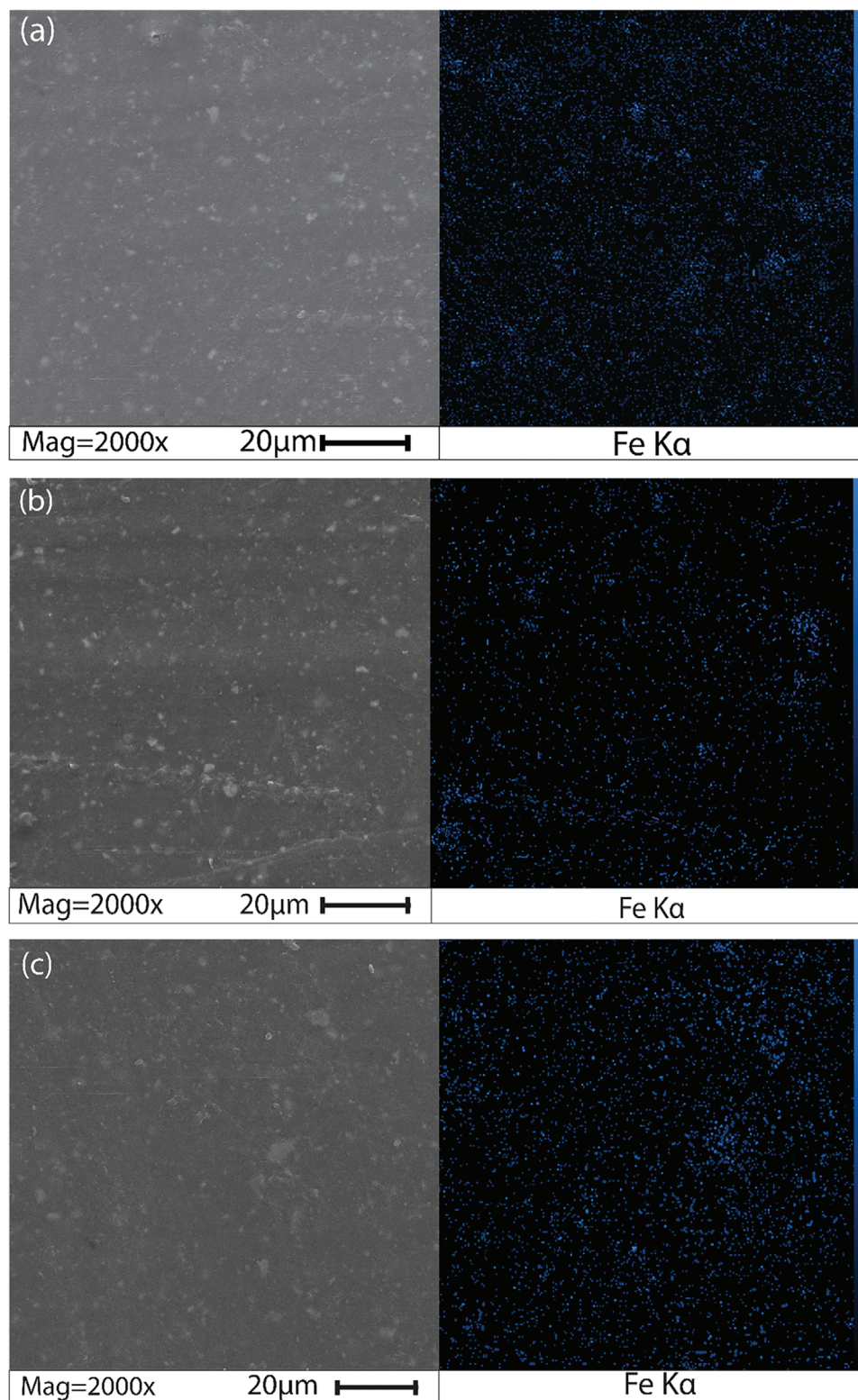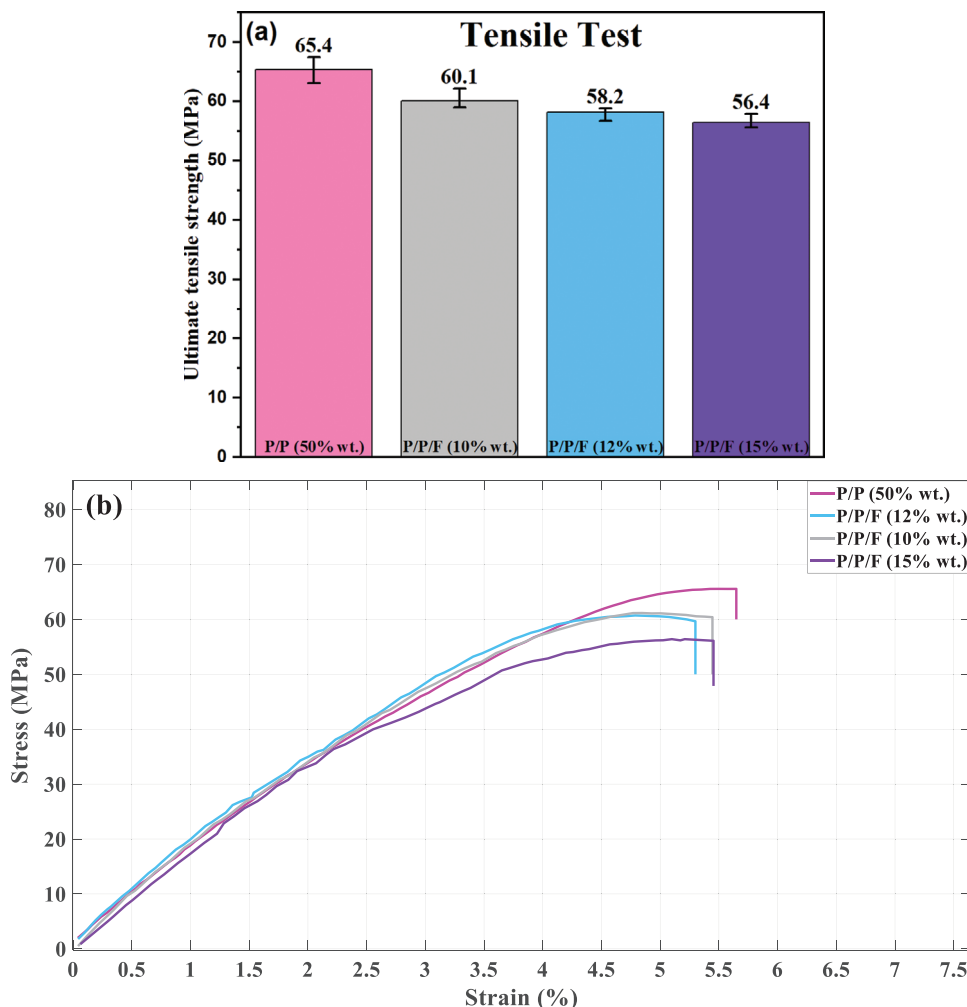

Figure 7. FE-SEM image of chemically etched PLA/PMMA (50/50 wt%) samples.

**ADVANCED
SCIENCE NEWS**

www.advancedsciencenews.com

{M} acro-
molecular
Materials and Engineering
Open Access

www.mame-journal.de

Figure 8. Elemental analysis and FE-SEM images of the MSMPs with a) 10 wt%, b) 12 wt%, and c) 15 wt% of Fe_3O_4 content and cross-sectional images of nanocomposites.

2400090 (8 of 13)

**ADVANCED
SCIENCE NEWS**

www.advancedsciencenews.com

[M] acro-
molecular
Materials and Engineering

www.mame-journal.de

Figure 9. a) Ultimate tensile strength and b) stress–strain curves of the magnetic nanocomposites.

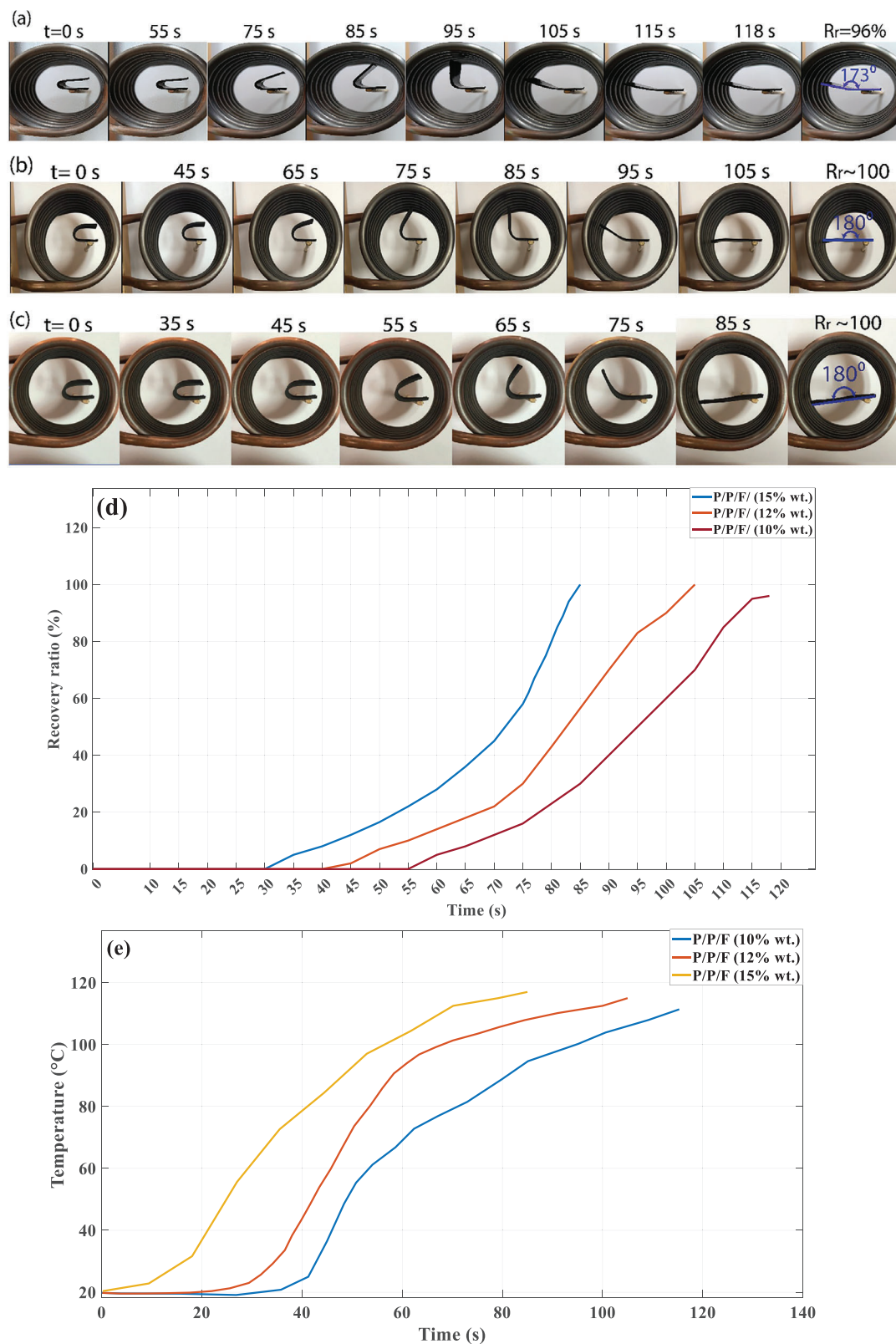of the material indicates that the phase morphology is homogeneous as desired.

3.3. Tensile Test

Shape memory polymers are mainly used as actuators, sensors, and scaffolds in the biomedical field and robotic devices. One of the main requirements in these applications is to have good mechanical strength. The ultimate tensile strength and stress-strain curves of the materials are presented in **Figure** 9a,b respectively. According to the results and based on the agglomerated zones (with maximum diameter of 3μ) shown in Figure 8a–c, the mechanical strength decreased slightly. Despite the slight reduction in toughness and tensile strength, the magnetic nanocomposites are mechanically robust and are suitable for the aforementioned applications.

3.4. Physical Interpretations of Magnetic Shape Memory Effect

According to DMTA and FE-SEM results, PLA and PMMA phases have robust interactive relations even when nanoparticles are in-

corporated in these blends. In the study conducted by Shi et al.[50] broad glass transition of blends is known as a collection of individual glass transitions that each corresponds to an individual shape memory element in nano-domains; therefore, it can be inferred that high T_g and low T_g nano-domains with different amounts of oriented PLA/PMMA can be selectively activated during the shape recovery process. In this respect, three different mechanisms happen when the nanocomposites are placed in a high-frequency alternating magnetic field. At low switch temperatures (≈60 to 75 °C), PLA-rich nanodomains act as the soft domains and as a result, PLA chains are responsible for shape changes. At temperature ranges between 75 and 85 °C highly entangled PLA and PMMA chains are responsible for shape changes and at higher switch temperatures (near 90 °C) only PMMA chains in PMMA-rich domains are thermally activated. In fact, the peak observed in the tanδ curve for PLA/PMMA/Fe_3O_4 blends are the switching temperatures for interconnected PLA/PMMA chains. Based on the given information, the stretching temperature was selected at 95 °C to make sure all chains are involved in shape-changing process. Nanoparticles can act as the reinforcing agents within the MSMP matrix. They provide physical constraints that assist in maintaining the

**ADVANCED
SCIENCE NEWS**

www.advancedsciencenews.com

acro-
olecular
**Materials** and **Engineering**
Open Access

www.mame-journal.de

Figure 10. Shape recovery time for nanocomposites with a) 10 wt%, b) 12 wt%, c) 15 wt% of Fe_3O_4 content, d) recovery ratio, and e) recorded temperature of the specimens versus time.

**ADVANCED
SCIENCE NEWS**

www.advancedsciencenews.com

{M}acro-molecular
Materials and Engineering
Open Access

www.mame-journal.de

temporary shape. This reinforcement effect is responsible for a higher shape fixity ratio by preventing excessive relaxation of the polymer chains and supporting the fixation of the deformed configuration. The shape memory tests in alternating magnetic field with the aforementioned conditions were conducted and the results are demonstrated in **Figure 10**. As it can be seen all samples exhibited perfect shape fixity ($\approx$100%). Magnetic nanocomposite with 15 wt% of Fe_3O_4 had the best performance in shape recovery time, shape fixity, and shape recovery ratio (Movie S1, Supporting Information). The observed trends also indicate that higher quantities of Fe_3O_4 correspond to a more rapid shape recovery. It is logical since the higher content of Fe_3O_4 causes better thermal conductivity between nanoparticles. The underlying mechanism of this phenomenon in an alternating magnetic field is that the heat is induced in magnetic nanoparticles and the well-dispersity of nanoparticles helps better conduction inside the polymer matrix. Figure 10d demonstrates the effect of nanoparticles content on the recovery ratio of MSMPs. It is evident that heat is more effectively transferred in nanocomposites with a higher content of Fe_3O_4. The temperature versus time curves in Figure 10e show almost the same trend of heat in samples. These curves indicate that specimens with higher amount of Fe_3O_4, recover their permanent shapes in shorter time as the nanoparticles are closer and heat conduction happens much faster. It also should be noted that the frequency of the magnetic setup is fixed at f = 100 kHz and the change in the amount of Fe_3O_4 does not have significant effect on the frequency of the test since its amount change in different nanocomposite is negligible. Hence, the results in Figure 10e prove the data plotted in Figure 10d.

Shape memory tests were also conducted in hot water at 95 °C, revealing a notable accelerated rate of shape recovery (shown in **Figure 11**). When immersed in hot water, the polymer chains reach the switching temperature in less than 6 s. It is important to note that when the MSMPs are heated, the presence of nanoparticles in MSMPs facilitates rapid and efficient heat transfer.

4. Potential Applications

SMP-based porous structures are highly suitable for biomedical field, especially bone fracture implants. Cellular materials are often composed of polymers or compounds that are biocompatible to minimize the risk of life-threatening chemical reactions. They are also designed with a specific level of porosity to help bone heal in a controlled manner. In this respect, biocompatibility, mechanical strength, and porosity are the main factors for designing these architectures. As discussed in the introduction section, PLA is a biodegradable polymer that has been employed in many research studies as bone scaffolds,[51–54] PMMA is a non-toxic biocompatible material with good chemical stability that can be recycled as well as Fe_3O_4. Given that the properties of the fabricated nanocomposites align with the tensile strength of human short bones and the contactless technique of the shape recovery process of the MSMPs which minimizes the risk of damaging the bone cells due to the remote activation process, the proposed nanocomposites can be an excellent choice for implant applications in addressing bone defects. As depicted in **Figure 12**, the holes caused by surgical operations can be filled with shape memory parts. The temporary shapes of these parts are designed to have minimum interaction with the bone tissue and are small
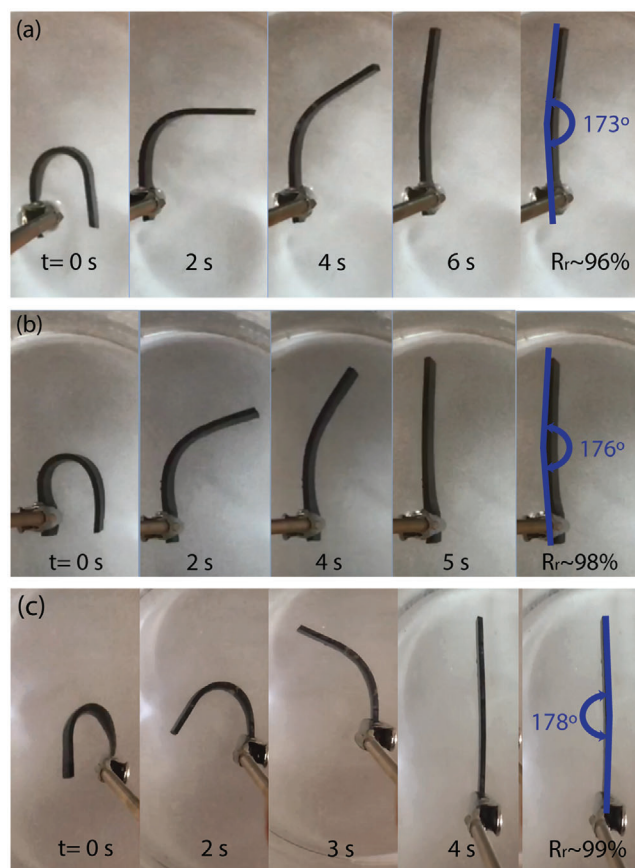

Figure 11. Direct heating shape memory tests of MSMPs with a) 10 wt%, b) 12 wt%, and c) 15 wt% of Fe_3O_4 content.

enough to be embedded inside the bone holes. Once they are implanted, the high frequency magnetic field is utilized to heat the nanoparticles inside the MSMPs. As discussed before, one of the advantages of this process is its remote actuation which minimizes the heat exchange between the MSMPs and its surroundings. According to Figure 12, two porous structures with 50% (Movie S2, Supporting Information) and 80% (honey-comb structure with) porosity as potential architectures for bone fracture implants were designed and 3D printed. Their remote actuation has been tested in the high frequency AC magnetic field and they both recovered their permanent shape within 82–85 s. In cases where bone regeneration is expected to take a considerable amount of time, the proposed nanocomposites can withstand mechanical loading till the healing process is completed. Figure 12 is a schematic representation of the suggested application for the proposed MSMPs.

5. Conclusion

In this study, magneto-thermo-responsive shape memory polymers based on PLA, PMMA, and Fe_3O_4 nanoparticles were successfully 4D printed for the first time. Homogeneous distribution of Fe_3O_4 nanoparticles in all nanocomposites was confirmed by FE-SEM. These nanoparticles did not influence the broadness of the thermal transition temperature and did not have a significant
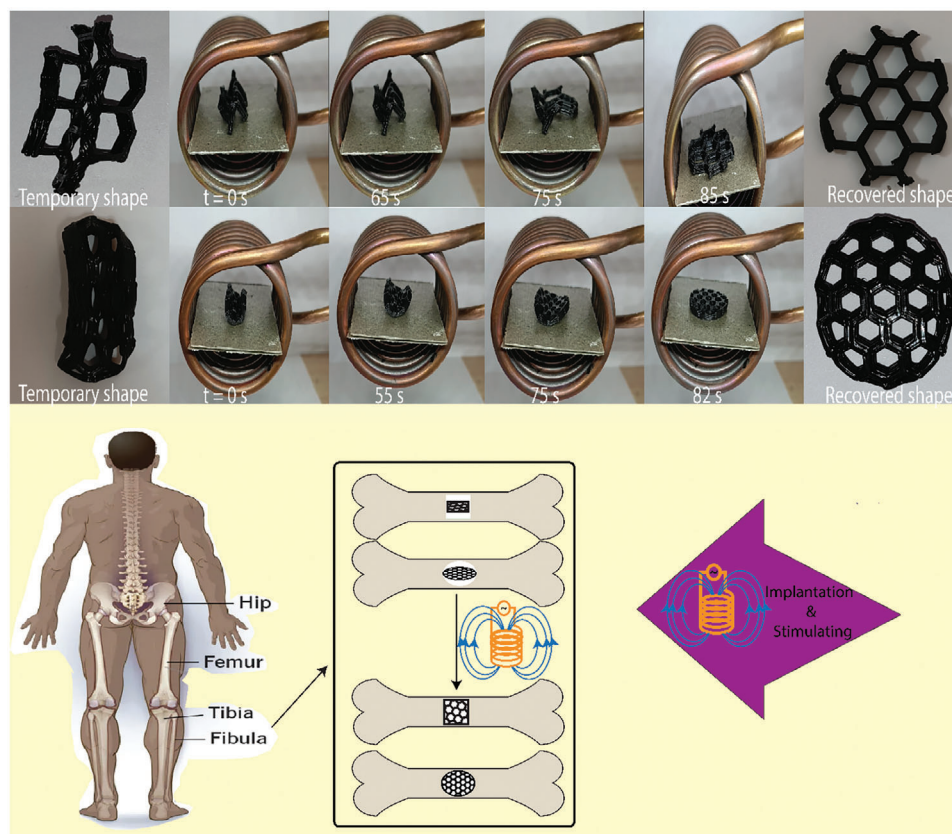
Figure 12. Schematic of potential application for the proposed MSMPs.

effect on the glass transition temperature of PLA/PMMA blends. The 3D-printed MSMPs displayed good mechanical strength but more importantly, these materials could be triggered remotely with a contactless method in an external magnetic field at f = 100 kHz thanks to the incorporation of Fe_3O_4 nanoparticles. The results demonstrated the high shape fixity ratios ($\approx$100%) with perfect shape recovery ratios ($\approx$100%) which were comparable with direct heating actuation. The higher content of Fe_3O_4 resulted in faster shape memory response and as observed in MSMPs with 15 wt% of Fe_3O_4, the shape recovery time was as fast as 85s as well as its porous structures. These remarkable characteristics along with the good mechanical strength ($\approx$60 MPa) of the proposed MSMPs, make them perfectly suitable for remote actuations including implants. Future studies on these materials can focus on developing bone scaffolds used specifically for minimally invasive surgical implants, biomimetic architectures, and actuators.

Supporting Information

Supporting Information is available from the Wiley Online Library or from the author.

Conflict of Interest

The authors declare no conflict of interest.

Data Availability Statement

The data that support the findings of this study are available from the corresponding author upon reasonable request.

Keywords

[1] W. Zhao, C. Yue, L. Liu, Y. Liu, J. Leng, *Adv. Healthcare Mater.* **2023**, *12*, 2201975.

[2] H. Liu, F. Wang, W. Wu, X. Dong, L. Sang, *Compos B Eng* **2023**, *248*, 110382.

[3] C. Linghu, Y. Liu, Y. Y. Tan, J. H. M. Sing, Y. Tang, A. Zhou, X. Wang, D. Li, H. Gao, K. J. Hsia, *Proc. Natl. Acad. Sci. USA* **2023**, *120*, e2221049120.

[4] P. Afshari, M. Pavlyuk, C. Lira, K. Katnam, M. Bodaghi, H. Yazdani Nezhad, *Macromol. Mater. Eng.* **2023**, *308*, 2300194.

[5] M. Lalegani Dezaki, M. Bodaghi, *Sens Actuators A Phys* **2023**, *349*, 114063.

[6] X. Q. Feng, G. Z. Zhang, Q. M. Bai, H. Y. Jiang, B. Xu, H. J. Li, *Macromol. Mater. Eng.* **2016**, *301*, 125.

**ADVANCED
SCIENCE NEWS**

www.advancedsciencenews.com

Macro-
molecular
Materials and Engineering
Open Access

www.mame-journal.de

[7] A. Enferadi, A. Ostadrahimi, G. Li, M. Baniassadi, M. Baghani, *Smart Mater. Struct.* **2024**, *33*, 055033.

[8] M. Y. Khalid, Z. U. Arif, R. Noroozi, A. Zolfagharian, M. Bodaghi, *J Manuf Process* **2022**, *81*, 759.

[9] C. A. Spiegel, M. Hackner, V. P. Bothe, J. P. Spatz, E. Blasco, *Adv. Funct. Mater.* **2022**, *32*, 2110580.

[10] T. Dayyoub, A. V. Maksimkin, O. V. Filippova, V. V. Tcherdyntsev, D. V. Telyshev, *Polymers (Basel)* **3511**, *14*, 2022.

[11] Z. Zhang, J. Du, W. Shan, T. Ren, Z. Lu, *Macromol. Mater. Eng.* **2021**, *306*, 2000508.

[12] X. Huang, M. Panahi-Sarmad, K. Dong, Z. Cui, K. Zhang, O. Gelis Gonzalez, X. Xiao, *Compos Part A Appl Sci Manuf* **2022**, *158*, 106946.

[13] T. Yang, W. Chen, J. Hu, B. Zhao, G. Fang, F. Peng, Z. Cao, *Appl. Compos. Mater.* **2022**, *29*, 473.

[14] Y. Bai, L. Ionov, *Mater. Chem. Front.* **2022**, *6*, 1218.

[15] S. Pisani, I. Genta, T. Modena, R. Dorati, M. Benazzo, B. Conti, *Int. J. Mol. Sci.* **1290**, *23*, 2022.

[16] Y. Xue, J. Lei, Z. Liu, *Polymer (Guildf)* **2022**, *243*, 124623.

[17] A. Shafe, C. D. Wick, A. J. Peters, X. Liu, G. Li, *Polymer (Guildf)* **2022**, *242*, 124577.

[18] M. Mattmann, C. De Marco, F. Briatico, S. Tagliabue, A. Colusso, X.-Z. Chen, J. Lussi, C. Chautems, S. Pané, B. Nelson, *Adv. Sci.* **2022**, *9*, 2103277.

[19] J. M. Avila, T. J. Cavender-Word, D. A. Roberson, *J. Polym. Environ.* **2023**, *31*, 3351.

[20] Y. Wang, X. Yu, R. Liu, C. Zhi, Y. Liu, W. Fan, J. Meng, *Compos Part A Appl Sci Manuf* **2022**, *160*, 107037.

[21] T. Li, J. Sun, J. Leng, Y. Liu, *J. Compos. Mater.* **2022**, *56*, 1725.

[22] M. Gastaldi, C. A. Spiegel, C. Vazquez-Martel, C. Barolo, I. Roppolo, E. Blasco, *Mol Syst Des Eng* **2023**, *8*, 323.

[23] Y. Wang, Y. Wang, Q. Wei, J. Zhang, *Eur. Polym. J.* **2022**, *173*, 111314.

[24] A. U. Vakil, M. Ramezani, M. B. B. Monroe, *Materials* **7279**, *15*, 2022.

[25] L. Fang, W. Yan, S. Chen, Q. Duan, M. Herath, J. Epaarachchi, Y. Liu, C. Lu, *Macromol. Mater. Eng.* **2023**, *308*, 2300158.

[26] M. Lalegani Dezaki, M. Bodaghi, *Int J Adv Manuf Technol* **2023**, *126*, 35.

[27] L. Fang, W. Yan, S. Chen, Q. Duan, M. Herath, J. Epaarachchi, Y. Liu, C. Lu, *Macromol. Mater. Eng.* **2023**, *308*, 2300158.

[28] S. Conti, M. Lenz, M. Rumpf, *J Mech Phys Solids* **2007**, *55*, 1462.

[29] , V. R. Nakum, K. M. Vyas, N. C. Mehta, *International Journal of Science and Engineering Applications* **2013**, *02*, 141.

[30] A. M. Davidson, *Magnetic Induction Heating of Superparamagnetic Nanoparticles for Applications in the Energy Industry*, Austin, **2012**.

[31] R. Hergt, R. Hiergeist, I. Hilger, W. A. Kaiser, Y. Lapatnikov, S. Margel, U. Richter, *J. Magn. Magn. Mater.* **2004**, *270*, 345.

[32] R. E. Rosensweig, *J. Magn. Magn. Mater.* **2002**, *252*, 370.

[33] R. U. Hassan, S. Jo, J. Seok, *J. Appl. Polym. Sci.* **2018**, *135*, 45997.

[34] P. R. Buckley, G. H. Mckinley, T. S. Wilson, W. Small, W. J. Benett, J. P. Bearinger, M. W. Mcelfresh, D. J. Maitland, *IEEE Trans. Biomed. Eng.* **2006**, *53*, 2075.

[35] I. Aaltio, F. Nilsén, J. Lehtonen, Y. L. Ge, S. Spoljaric, J. Seppälä, S. P. Hannula, *Mater. Sci. Forum* **2016**, *879*, 133.

[36] R. Mohr, K. Kratz, T. Weigel, M. Lucka-Gabor, M. Moneke, A. Lendlein, *Proc. Natl. Acad. Sci. USA* **2006**, *103*, 3540.

[37] C. M. Yakacki, N. S. Satarkar, K. Gall, R. Likos, J. Z. Hilt, *J. Appl. Polym. Sci.* **2009**, *112*, 3166.

[38] J. Puig, C. E. Hoppe, L. A. Fasce, C. J. Pérez, Y. Piñeiro-Redondo, M. Bañobre-López, M. A. López-Quintela, J. Rivas, R. J. J. Williams, *J. Phys. Chem. C* **2012**, *116*, 13421.

[39] C. Yao, M. Huang, G. Huang, S. He, X. Ma, Z. Li, Y. Wang, H. Liu, W. Liu, *ACS Appl. Eng. Mater.* **2023**, *1*, 2092.

[40] M. Imran Khan, M. M. Zagho, R. A. Shakoor, *Smart Polym. Nanocompos.* **2017**, 281.

[41] W. T. Nugroho, Y. Dong, A. Pramanik, J. Leng, S. Ramakrishna, *Compos B Eng* **2021**, *223*, 109104.

[42] Y. S. Alshebly, M. Nafea, M. S. Mohamed Ali, H. A. F. Almurib, *Eur. Polym. J.* **2021**, *159*, 110708.

[43] J. Puig, C. E. Hoppe, L. A. Fasce, C. J. Pérez, Y. Piñeiro-Redondo, M. Bañobre-López, M. A. López-Quintela, J. Rivas, R. J. J. Williams, *J. Phys. Chem. C* **2012**, *116*, 13421.

[44] M. Y. Razzaq, M. Anhalt, L. Frormann, B. Weidenfeller, *Mater. Sci. Eng., A* **2007**, *444*, 227.

[45] R. B. da Cunha, S. N. Cavalcanti, P. Agrawal, G. de Figueiredo Brito, T. J. A. de Mélo, *J. Appl. Polym. Sci.* **2023**, *140*, e54561.

[46] R. B. da Cunha, P. Agrawal, G. de Figueiredo Brito, T. J. A. de Mélo, *Shap Mem Superelasticity* **2023**, *9*, 601.

[47] J. Anakabe, A. Orue, A. M. Zaldua Huici, A. Eceiza, A. Arbelaiz, *J. Appl. Polym. Sci.* **2018**, *135*, 46825.

[48] C. Samuel, S. Barrau, J.-M. Lefebvre, J.-M. Raquez, P. Dubois, *Macromolecules* **2014**, *47*, 6791.

[49] F. J. Eshkaftaki, I. Ghasemi, *Polym. Bull.* **2018**, *75*, 4073.

[50] P. Shi, R. Schach, E. Munch, H. Montes, F. Lequeux, *Macromolecules* **2013**, *46*, 3611.

[51] N. Rodrigues, M. Benning, A. M. Ferreira, L. Dixon, K. Dalgarno, *Proc. CIRP* **2016**, *49*, 33.

[52] B. Zhang, L. Wang, P. Song, X. Pei, H. Sun, L. Wu, C. Zhou, K. Wang, Y. Fan, X. Zhang, *Mater. Des.* **2021**, *201*, 109490.

[53] R. Donate, M. Monzón, M. E. Alemán-Domínguez, *e-Polymers* **2020**, *20*, 571,.

[54] A. Gregor, E. Filová, M. Novák, J. Kronek, H. Chlup, M. Buzgo, V. Blahnová, V. Lukasová, M. Bartos, A. Necas, J. Hosek, *J. Biol. Eng.* **2017**, *11*, 31.